Thermal feedback in coaxial superconducting radio frequency cavities

Mattias McMullin,[1,2] Philipp Kolb,[1,*] Zhongyuan Yao,[1] Robert Laxdal,[1] and Tobias Junginger[2]
[1]TRIUMF, Vancouver, BC, Canada
[2]University of Victoria, Victoria, BC, Canada

(Received 20 April 2024; accepted 9 August 2024; published 3 September 2024)

The surface resistance of superconducting radio frequency (SRF) cavities depends on the strength of the applied rf field. This field dependence is caused by a combination of intrinsic losses and the extrinsic thermal feedback (TFB) effect. To test theories of intrinsic field dependence, the extrinsic part must be compensated for when analyzing experimental data from SRF cavity tests. Performing this compensation requires knowing thermal parameters that describe heat flow in the cavity walls. The relevant thermal parameters have been measured in the case of superfluid helium, below 2.177 K, but no detailed measurements have yet been reported for cooling of niobium surfaces in normal fluid helium baths. Because of this, the impact of TFB on the field dependence at temperatures near 4.2 K is unknown. In the present study, we report measurements of normal fluid helium boiling from niobium surfaces and its dependence on the orientation of the boiling surface and bath temperature. These measurements are used to create a finite-element model of heat transfer in cavities from TRIUMF's coaxial test program. This tool is then used to compensate for TFB when analyzing a range of datasets from this program. Results are presented showing that TFB has a weak impact for the temperatures of 2.0 and 4.2 K, where SRF cavities are usually operated, but it is an important effect at intermediate temperatures.

DOI: 10.1103/PhysRevAccelBeams.27.092001

I. INTRODUCTION

Superconducting radio frequency (SRF) cavities are used to provide transfer energy to the particle beam in many modern particle accelerators. Applications include heavy-ion accelerators like ISAC-II at TRIUMF [1] or FRIB [2] as well as electron accelerators like LCLS-II [3] or EUXFEL [4]. SRF cavities are used instead of normal conducting cavities in applications where both high accelerating gradients and low power dissipation are essential. Due to the high costs of the helium cryogenics systems required to operate SRF cavities, a major focus of research in the field is on further reducing power dissipation to reduce the load on these systems.

The power dissipated in an SRF cavity is roughly proportional to the surface resistance. In the limit of low rf field strength, the surface resistance can be split into two parts:

$$R_s(\omega, T) = R_0 + R_{\mathrm{BCS}}(\omega, T), \tag{1}$$

where ω is the rf angular frequency, T is the rf surface temperature, R_0 is the temperature-independent residual resistance, and $R_{\mathrm{BCS}}(\omega, T)$ is the temperature-dependent surface resistance derived in the weak-field limit of the BCS theory of superconductivity [5]. Since it has no closed form, $R_{\mathrm{BCS}}(\omega, T)$ must be evaluated using numerical codes like SRIMP [6], but a useful approximation is given by [7]

$$R_{\mathrm{BCS}}(\omega, T) = \frac{A\omega^2}{T}\exp\left(-\frac{\Delta}{k_B T}\right), \tag{2}$$

where A is a constant that depends on material properties and Δ is the superconducting energy gap.

The surface resistance is inferred from measurements of the unloaded quality factor Q_0, defined as

$$Q_0 = \frac{\omega U}{P}, \tag{3}$$

where U is the total energy stored in the fields in the cavity and P is the total power dissipation in the cavity, which is given by

$$P = \int_S \frac{1}{2} R_s H^2 \, dS, \tag{4}$$

*Contact author: kolb@triumf.ca

where S is the rf surface of the cavity. If the surface resistance is uniform on the rf surface, then it can be found from a measurement of Q_0 by

$$R_s = \frac{G}{Q_0}, \tag{5}$$

where G is a constant that depends on the cavity geometry. If R_s is not uniform, then G/Q_0 can be treated as a measurement of the average surface resistance.

The most common type of SRF cavities used in accelerators are 1.3 GHz elliptical cavities. These cavities are operated in superfluid helium near 2.0 K in order to keep $R_{\mathrm{BCS}}(\omega, T)$ at an acceptable level. Coaxial cavities used in heavy ion accelerators often have resonant frequencies below 500 MHz. Because of the quadratic dependence of $R_{\mathrm{BCS}}(\omega, T)$ on ω, $R_{\mathrm{BCS}}(\omega, T)$ is much lower than for 1.3 GHz elliptical cavities, so these lower frequency cavities are often operated at 4.2 K. Operation at 4.2 K is desirable because it eliminates the need for subatmospheric pumping required to cool helium below 4.2 K, and therefore, reduces the cost and complexity of the cryogenics systems. Most fundamental research in the field is based on 1.3 GHz elliptical cavities, but it is essential to extend this attention to coaxial cavities operating in 4.2 K normal fluid helium in order to pave the way for future highly efficient accelerator designs.

The approximation of Eqs. (1) and (2), which is only valid in the limit of low field strength, implies that the surface resistance is independent of the applied field. In reality, R_s typically increases with the rf field, which challenges efforts to build accelerators with both high gradients and low power dissipation. Some novel treatments have been shown to reverse this dependency for electropolished cavities at frequencies above 1 GHz [8,9], a useful effect that is now being exploited in the LCLS-II-HE project [10]. The physical mechanisms that determine whether R_s increases or decreases with the rf field and the strength of this dependency, however, remain obscure. Some proposed fundamental theories explain field-dependence as the result of percolation effects [11] or of the modification of the local quasiparticle density of states [12].

In addition to these proposed mechanisms, which are related to the intrinsic properties of the rf surface, field dependence is also caused by the extrinsic *thermal feedback* (TFB) effect [13]. A brief summary is as follows: during an rf measurement, heat is dissipated within a thin layer (~100 nm) on the rf surface of the cavity. The niobium walls have finite thermal conductivity and the cooling at the niobium-helium interface is imperfect, so a thermal gradient forms between the rf surface and the helium bath, as shown in Fig. 1. The strong temperature dependence of the surface resistance then causes the dissipated rf power density

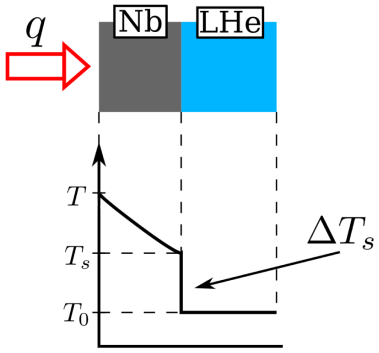

FIG. 1. Cross section showing the temperature gradient across the wall of an SRF cavity [14]. Here T is the rf surface temperature, T_s is the temperature of the outer surface of the cavity, and T_0 is the temperature of the helium bath.

$$q = \frac{1}{2} R_s H^2 \tag{6}$$

to rise, which further increases the thermal gradient to establish a feedback loop. As long as the cooling is sufficient to prevent a cavity quench, the feedback loop will reach an equilibrium condition where the rf surface temperature T is somewhat larger than the bath temperature T_0. This equilibrium temperature difference increases with the rf field strength. Therefore, the surface resistance increases with the rf field because of TFB in addition to any intrinsic field dependence.

In order to understand the fundamental physics involved in the field-dependence of R_s, it is necessary to know what portion of measured field dependence can be attributed to TFB as opposed to intrinsic effects. Since it is not possible to measure the temperature distribution on the rf surface during an rf measurement, the effects of TFB must be estimated using a physical model of heat flow in the cavity walls. A critical component of any such model is the heat conductance through the Nb-LHe interface. In the case of superfluid helium, when $T_0 < 2.177$ K, this interface heat conductance is known as the *Kapitza conductance* and has been studied for Nb-LHe interfaces [15,16]. These measurements have been previously used to thoroughly study TFB in the superfluid regime [17,18].

In normal fluid helium, measurements of heat transfer at the Nb-LHe interface have been made using materials like copper and silver [19,20]. One study [21] also reported results for niobium, but due to limitations of the apparatus the measurements were of unknown precision and did not provide any information about the effect of the orientation of the boiling surface. Studies that use estimates for heat conductance based on data for boiling from non-niobium surfaces have found that TFB is not a strong enough effect to explain *all* measured field dependence [13,22,23], but no study to date has offered a method for determining *how much* field dependence should be attributed to TFB.

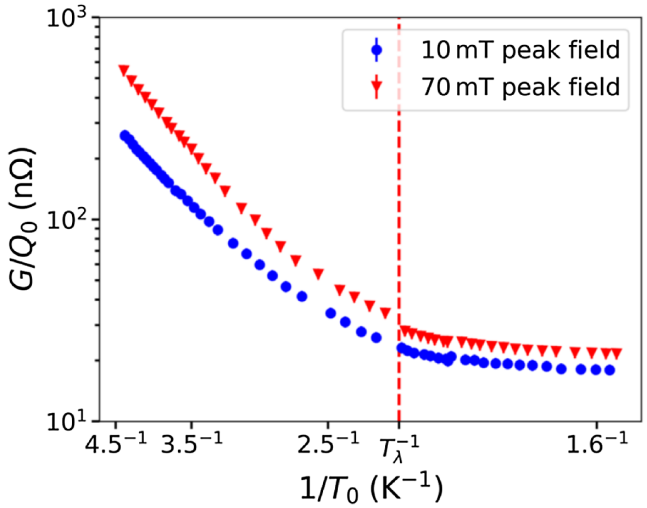

FIG. 2. Average surface resistance G/Q_0 vs inverse bath temperature $1/T_0$ measured in a half-wave resonator baked at 400°C with an rf frequency of 778 MHz. Note the jump in surface resistance at T_λ for $B_p = 70$ mT.

TFB has previously been studied only in elliptical cavities. The coaxial test cavity program at TRIUMF, which is detailed in [24], studies the fundamental physics of surface resistance in coaxial cavities at rf frequencies between 200 and 1200 MHz and at temperatures from 1.5 to 4.5 K. Data from this program show signs that TFB is a non-negligible effect in normal fluid helium. Below $T_\lambda = 2.177$ K, the surface resistance drops abruptly, as shown in Fig. 2, and the size of the drop grows with the rf field strength. This drop has been observed in other studies [23,25] and is believed to occur because the helium bath enters a superfluid state and cooling is significantly enhanced, substantially mitigating TFB. The presence of the drop, therefore, raises the question of how strongly TFB impacts measurements throughout the entire range of bath temperatures above T_λ.

The present study begins in Sec. II with a measurement of liquid helium boiling from niobium surfaces. The newly measured parameters are used in Sec. III to create a finite-element model of heat flow in the coaxial cavities. This FEA tool is then used in Sec. IV to reveal the impact of TFB in the coaxial cavity datasets and the results of the study are summarized in Sec. V.

II. Nb-LHe BOILING MEASUREMENTS

The heat flux q through a surface cooled by liquid at its boiling point is determined by the temperature difference between the surface and the liquid, ΔT_s. At very low heat fluxes, the surface is cooled by natural convection and q and ΔT_s are roughly proportional to one another. As the heat flux increases, bubbles start to form at nucleation sites, marking the start of the nucleate boiling regime. As more nucleation sites become active, heat transfer grows more efficient (lower ΔT_s for a given q) until the density of active nucleation sites reaches a maximum. If the heat flux is made sufficiently high, the bubbles will coalesce into a film. This regime, film boiling, is characterized by very poor heat transfer and is not relevant to the performance of unquenched SRF cavities. If the heat flux is instead decreased after reaching the developed nucleate boiling regime, some nucleation sites will remain active until very low heat fluxes. Heat transfer will be more efficient for decreasing heat flux than for increasing, creating some degree of hysteresis in the relationship between q and ΔT_s.

The relationship between q and ΔT_s in any regime can be described by the empirical formula

$$q = a(\Delta T_s)^n, \tag{7}$$

where a and n are the constants that depend on the regime of heat transfer as well as on properties of the working fluid and heater surface. For heat transfer by natural convection in any fluid, the exponent n is near 1, and for nucleate boiling in liquid helium, n has been measured in the range 1–3 [19,26].

The relationship between q and ΔT_s described above is called a *boiling curve* [27]. Boiling curves are qualitatively similar for any pairing of working fluid and surface, but a quantitative description of heat transfer depends on the fluid being used, its temperature, and characteristics of the boiling surface like material, roughness, shape, and orientation. In the case of TRIUMF's coaxial SRF cavities during cooldown measurements, the working fluid is saturated liquid helium between 2.177 and 4.5 K and the surface is substantially flat, high-purity niobium sheet.

To produce a suitable sample for the boiling measurement, a sheet of 2.1 mm thick rolled niobium with RRR > 250 was bonded to a 1 in. thick C10100 copper base plate by explosion welding [28]. A cylinder with a diameter of 34 mm was cut from this bonded block and the surface was turned on a lathe to remove irregularities from the welding process. Unlike TRIUMF's coaxial cavities, which undergo a range of different heat treatments at or below 800 °C, the sample was not heat treated, and therefore, has a different thermal conductivity than the cavities [29]. This factor was neglected because the sample was used for measurements in the normal fluid regime, where the thermal conductivity does not strongly affect the boiling performance unless the surface is highly polished [30].

A hole was drilled in the copper block for mounting a thermometer, as shown in Fig. 3. Both the copper block and helium bath temperatures are measured using Lakeshore Cernox [31] sensors. The sample cylinder was soldered to a 2.75 in. CF flange with a small portion of the sides of the cylinder exposed on the top of the flange. The exposed portion of the sides was covered with a PTFE ring to prevent contact with helium, as shown in Fig. 4. The helium chamber in which the sample is mounted is constructed from rotatable

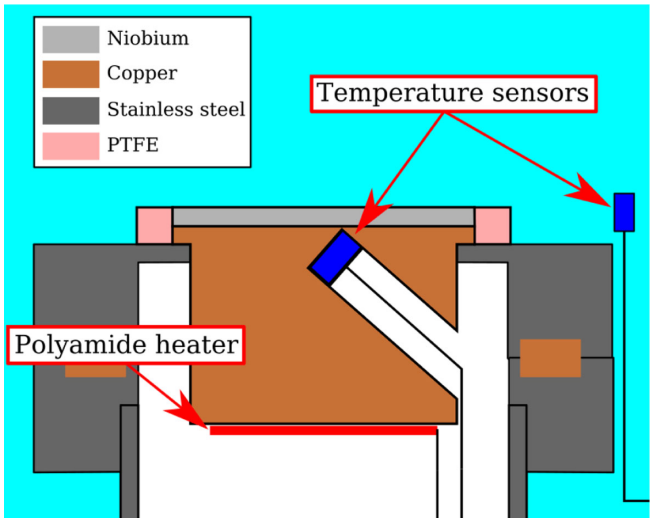

FIG. 3. Schematic of the test setup for boiling curve measurements [14].

FIG. 4. A sample flange with the PTFE ring and Cernox sensor installed.

CF fittings, enabling control of the orientation of the boiling surface during the setup of a measurement.

During the measurement, heat is applied by a polyamide heater on the bottom of the copper block. The thick copper backing smooths out temperature variations across the niobium disc and functions as an isotherm for measuring the temperature of the niobium at the Nb-Cu weld. The total heat dissipated by the polyamide heater can be precisely controlled. Most of the heater power passes through the niobium surface into the helium bath, but some portion is lost to the system, primarily through the mounting flange. The system heat losses were quantified by a calibration measurement in which the niobium surface was covered by a thick PTFE block. By covering the surface, all heater power is assumed to be lost to the system. A relationship between the copper block temperature and the system heat losses was established by varying the heater power and recording the steady-state response of the sample temperature sensor.

Boiling curves are measured by ramping the heater power up and down in discrete steps and letting the system settle to a steady state at each step. The range of heater powers is chosen to match the range of heat fluxes relevant to coaxial cavity data, which are less than 500 $\mathrm{W/m^2}$. After subtracting the calibrated system heat losses, the heat flux q through the niobium surface is known at each step.

The temperature of the boiling surface is lower than the temperature measured by the thermometer in the copper block (see Fig. 3) by an amount equal to the sum of two thermal gradients: one across the niobium disc and another across the Nb-Cu explosion weld interface. The first of these gradients is estimated using literature data for niobium thermal conductivity [32]. The second gradient, $\Delta T_{\mathrm{Nb/Cu}}$, is estimated by

$$\Delta T_{\mathrm{Nb/Cu}} = q \cdot R_{\mathrm{Nb/Cu}}, \tag{8}$$

where $R_{\mathrm{Nb/Cu}}$ is the interfacial thermal resistance at the weld, which is taken as the phonon radiation limit value of 0.3 $\mathrm{cm^2\,K/W}$ [33].

Together with the readings from the bath temperature sensor, this produces a ΔT_s corresponding to each q in the ramp, yielding a boiling curve. An example of a boiling curve measured in this way is shown in Fig. 5.

Boiling curves were measured at bath temperatures of 4.2, 2.5, and 2.2 K. The sample housing was rotated to measure boiling curves at these temperatures with the surface normal facing upward, sideways, and downward, although no 2.2 K curves were measured with the Nb sample surface facing upward. Within the same cooldown, boiling curves at one temperature were typically collected two or three times and were always found to be repeatable within experimental uncertainties.

For a given heat flux q, the steady-state ΔT_s is larger for lower bath temperature (see Fig. 6), meaning that heat transfer is less efficient at lower temperatures. Figure 7

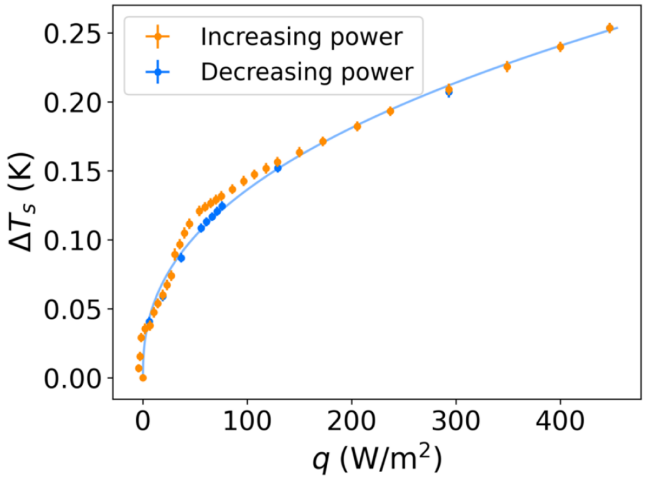

FIG. 5. A boiling curve at 4.2 K with the surface normal pointing upward. This curve displays the most hysteresis of any boiling curves collected in our measurements. The curve fit is from Eq. (7) with parameters listed in in Table I for the orientation "up".

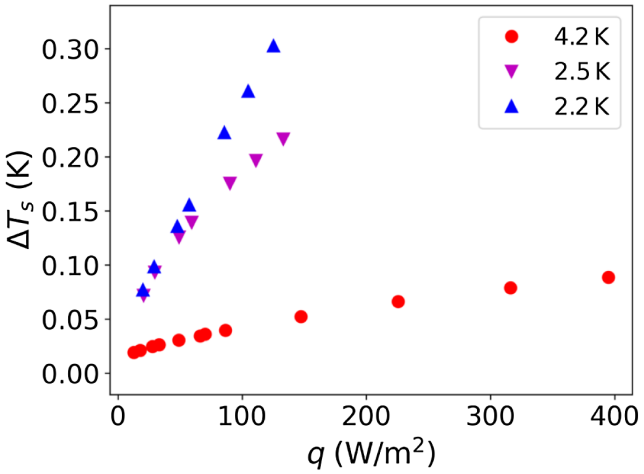

FIG. 6. Decreasing portions of curves taken at 4.2, 2.5, and 2.2 K from the dataset "side" in Table I.

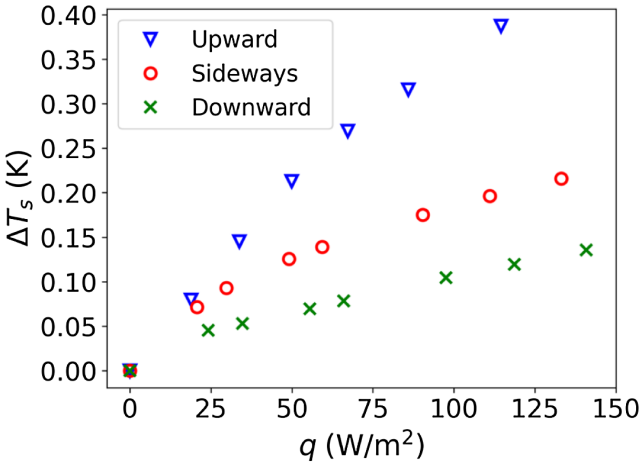

FIG. 7. Decreasing portions of curves taken at 2.5 K for three orientations of the surface normal.

shows that as the surface is rotated to the downward facing position, heat transfer becomes more efficient. This commonly observed feature in boiling curve studies is usually attributed to the increased disturbance of the superheated liquid layer by bubbles sliding along the surface [34].

Hysteresis was observed in only a few boiling curves, and the width of hysteresis was small and limited to a narrow range of heat fluxes, as shown in Fig. 5. Therefore, the hysteresis in the transition between the natural convection and nucleate boiling regimes was neglected in all TFB calculations below. Because the peak dissipated heat fluxes in TRIUMF's coaxial cavity data are on the order of 10^2 W/m^2, it is also assumed below that heat is transferred via developed nucleate boiling. To obtain a continuous interpolation of the nucleate boiling data, the decreasing heat flux data, which represents the developed nucleate boiling regime, were fit to Eq. (7). The fitting process only included data at heat fluxes higher than the linear natural convection regime, which was judged to be above 50 W/m^2 at 4.2 K and above 30 W/m^2 at 2.2 and 2.2 K. Table I shows the resulting fit parameters for representative boiling curves from each orientation.

TABLE I. List of fit parameters for measured boiling curves.

Orientation	T_0 (K)	a (W/m^2 K^n)	n
Up	4.26	12900 ± 300	2.44 ± 0.02
	2.54	400 ± 20	1.33 ± 0.05
Side	4.24	39000 ± 2000	1.89 ± 0.02
	2.53	2200 ± 200	1.83 ± 0.06
	2.24	520 ± 30	1.19 ± 0.04
Down	4.25	20800 ± 700	1.44 ± 0.01
	2.53	2500 ± 200	1.43 ± 0.04
	2.25	1700 ± 100	1.48 ± 0.04

The data collected here for the sideways orientation are in good agreement with previously reported data on boiling from silver surfaces [20]. No comparable data have been reported for the other two orientations. As it is seen by comparing the fit parameters listed in Table I for the curves measured at 4.2 K, the gap between the curve in the upward orientation and the curves measured in the other two orientations is larger than in the 2.5 K curves, which are shown in Fig. 7. This was most likely caused by a change in the cryogenics setup between measurements. This curve was not remeasured because it is of marginal importance to describing heat transfer in coaxial cavities, where the most of the power is dissipated on the sideways-oriented inner conductor.

III. FINITE-ELEMENT METHODS

The main goal of TRIUMF's coaxial program is to understand how the surface resistance depends on field strength, temperature, rf and surface treatment in coaxial cavities. After applying the desired surface treatment to the chosen cavity (QWR or HWR), a cavity test begins with lowering the cavity into a helium cryostat and cooling it to about 4.5 K. After thermalization, the cavity is excited in the chosen rf mode and the quality factor Q_0 is measured as a function of peak surface magnetic field B_p. This process is repeated while cooling down the helium bath to below 2 K. The result is a collection of Q_0 vs B_p curves at a range of bath temperatures with a single rf frequency. These measurements are then repeated for the other cavity modes.

Trends in the dependence of the surface resistance on temperature, rf frequency, and field strength are analyzed by fitting models of surface resistance to a chosen portion of coaxial cavity data. To find the best fit parameters, fitting routines require a function that returns a Q_0 prediction at a given set of (ω, T_0, B_p) with a known surface resistance function $R_s(\omega, T, B)$. To create such a prediction function that accounts for the full field nonuniformity in coaxial

cavities as well as the effects of TFB, including the dependence of heat transfer on surface orientation, we exploited finite-element methods.

Suppose that the rf surface resistance of a cavity is described everywhere by a known function $R_s(\omega, T, B)$ and that T_0, ω, and B_p are given as well. The total energy U in Eq. (3) can be calculated from B_p, but the total power dissipation P as given by Eq. (4) cannot be found without knowing the distribution of R_s on the cavity surface at thermal equilibrium. Since the field distribution and the surface resistance function $R_s(\omega, T, B)$ are known, this only requires finding the temperature distribution on the rf surface at thermal equilibrium.

To simplify the simulation, the bottom endplates of the cavities are treated as if they did not have the ports shown in Fig. 8. Because the magnetic field is near zero on the bottom endplate of the QWR, this simplification does not significantly affect the power dissipation calculations for that cavity. In the HWR, the magnetic field near the ports does not vanish, but simulations showed that neglecting the ports introduces an error of less than 1% when calculating the total dissipated power [35]. With this simplification, both the HWR and QWR have full cylindrical symmetry around the vertical axis. The equilibrium temperature distribution is found by solving the steady-state heat equation

$$\nabla^2 T = 0 \tag{9}$$

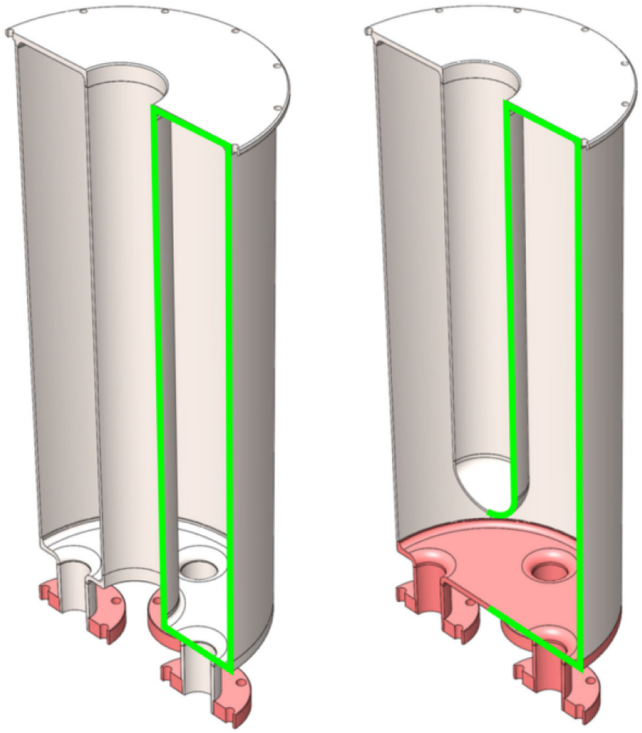

FIG. 8. HWR (left) and QWR (right) test cavities from TRIUMF's coaxial program. The 2D solution domain for the finite-element problem is highlighted in green.

in a 2D cross section of the cavity walls, as shown in Fig. 8. The boundary conditions are of two kinds. For the rf surface, the heat flux is given by Eq. (6). On the helium side, Eq. (7), together with the fit parameters listed in Table I, provides the relation between the cavity exterior surface temperature and heat flux through the Nb-LHe interface.

Since the boiling curves were only measured at three bath temperatures, the data are interpolated to define the helium side boundary condition at any $T_0 > T_\lambda$. For example, when considering a piece of the cavity wall exterior that is oriented sideways with $T_0 = 3.0$ K with some known ΔT_s, the heat flux at that portion of the boundary is found by evaluating Eq. (7) for the $T_0 = 2.53$ K and $T_0 = 4.24$ K "side" boiling curves (Table I) and linearly interpolating between these two heat fluxes based on the bath temperature.

The 2D heat equation problem described above is solved computationally using finite-element methods. Further details are given in [35]. In particular, the Ritz-Galerkin method of weighted residuals [36] is adopted. In this scheme, the 2D solution domain is broken up into a mesh of triangular finite elements. Instead of finding a continuous temperature distribution, the problem is reduced to finding the temperature at the vertices of all triangles in the mesh. This is done by solving a single sparse matrix equation for $\mathbf{T}$, a vector containing the temperatures of all these vertices:

$$(\mathbf{M} - \mathbf{B}) \cdot \mathbf{T} = \mathbf{p}_{\mathrm{rf}} + \mathbf{b}. \tag{10}$$

Here $\mathbf{M}$ is a matrix that depends only on the geometry of the mesh, $\mathbf{p}_{\mathrm{rf}}$ is a column vector determined by the distribution of heat flux on the rf surface, and $\mathbf{B}$ and $\mathbf{b}$ are a matrix and column vector, respectively, calculated from the distribution of heat flux on the surface exposed to helium. The thermal conductivity sets the scale of the elements of $\mathbf{p}_{\mathrm{rf}}$, $\mathbf{B}$, and $\mathbf{b}$. It is assumed that the thermal conductivity is uniform throughout the cavity and is calculated using the parameterization of [32]:

$$\kappa(T_0)\,(\mathrm{W/K\,m}) = 0.7 e^{1.65T_0 - 0.1T_0^2}. \tag{11}$$

The quality factor at thermal equilibrium is found using an iterative approach. Equation (10) is solved to find $\mathbf{T}$ and this new temperature distribution is used to recompute the matrices $\mathbf{p}_{\mathrm{rf}}$, $\mathbf{B}$, and $\mathbf{b}$. This process is repeated until the total dissipated power P converges, which also yields an equilibrium temperature distribution as shown in Fig. 9. Equation (3) then gives the quality factor Q_0.

IV. DATA ANALYSIS

To analyze the effects of TFB on field-dependence in TRIUMF's coaxial cavity datasets, the finite-element tool described in the previous section is used to fit the datasets with a model of surface resistance that parameterizes the

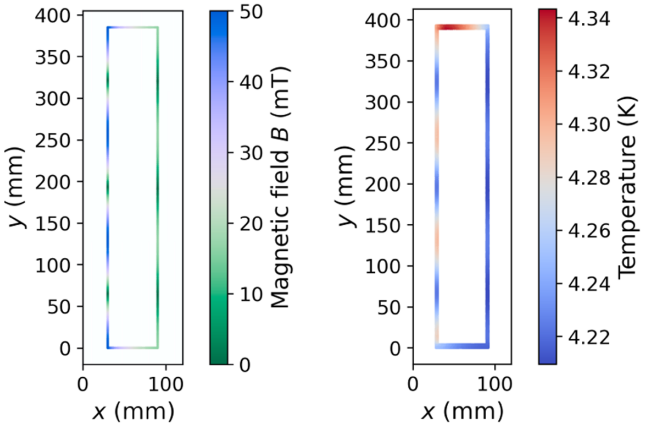

FIG. 9. Magnetic field (left) and equilibrium temperature (right) distributions for the 1166 MHz mode of the HWR on the domain shown in Fig. 8 with $B_p = 50$ mT and $T_0 = 4.2$ K. Note that despite the symmetry of the magnetic field, the temperature distributions on the top and bottom plates are different due to the orientation dependence of boiling heat transfer shown in Fig. 7.

field dependence. The field dependence in the coaxial cavity datasets is described well by

$$R_s(\omega, T, B) = \left(1 + \alpha\left|\frac{B}{B_0}\right|\right) R_0 + \left(1 + \gamma\left[\frac{B}{B_0}\right]^2\right) R_{\mathrm{BCS}}(\omega, T), \quad (12)$$

where $B_0 = 100$ mT is chosen to normalize the values of α and γ. In Eq. (12), $R_{\mathrm{BCS}}(\omega, T)$ is given by Eq. (2), with the temperature dependence of Δ approximated as [37]

$$\Delta(T) = \Delta_0 \sqrt{\cos\left(\frac{\pi}{2}\left[\frac{T}{T_c}\right]^2\right)}, \quad (13)$$

where T_c is the critical temperature, with $T_c = 9.2$ K for niobium.

In Eq. (12), two parameters (α and γ) quantify the field dependence and three parameters (A, Δ_0, and R_0) define the surface resistance in the low-field limit. The linear field dependence of the residual resistance comes from losses related to flux trapping [38] and the quadratic field dependence of the temperature-dependent surface resistance may be explained by models of pair-breaking [39] or percolation effects [11].

For a given coaxial cavity dataset, the low-field resistance parameters (A, Δ_0, and R_0) are found by fitting Eq. (12) to the lowest field ($B_p = 10$ mT) data while keeping $\alpha = \gamma = 0$ fixed and assuming no TFB (Fig. 10). This fit is constrained so that the fit exactly matches the lowest temperature point. The constraint ensures that the correct function $R_{\mathrm{BCS}}(T)$ is used, a point that will be explained further below.

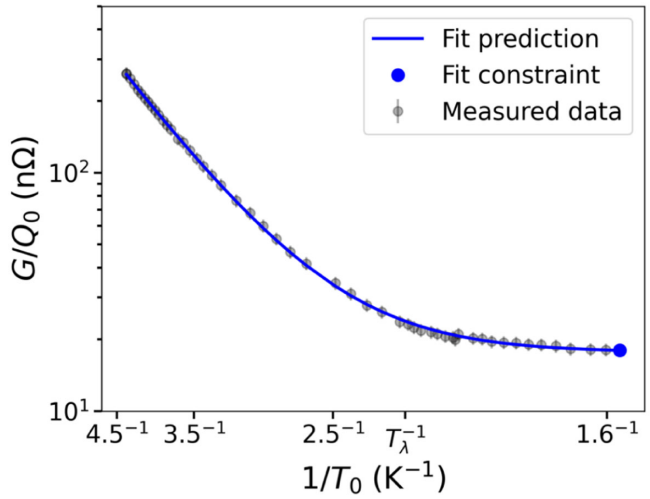

FIG. 10. Data from the 778 MHz mode of the 400°C baked HWR, showing a fit of Eq. (12) to the 10 mT data with no field dependence or TFB, constrained to match the Q_0 of the lowest temperature point.

In the lowest temperature measurements of a coaxial cavity test (T_0 near 1.5 K), the surface resistance is dominated by the temperature-independent part. The field dependence of the surface resistance in this regime can, therefore, be mostly attributed to the temperature-independent part, which gives a method for finding α in Eq. (12): the low field-resistance parameters (A, Δ_0, and R_0) are held fixed and α is fit to the lowest temperature Q vs B_p curve in the dataset, as shown in Fig. 11, while keeping $\gamma = 0$. In the coaxial cavity datasets, α lies between 0.2 and 1.1 but no clear dependence on rf frequency or surface treatment could be determined.

Once α has been fit, the parameter γ may be fit for any Q-curve in the dataset. For a given Q-curve, the residual resistance R_0 is held fixed to the value at which it was fit

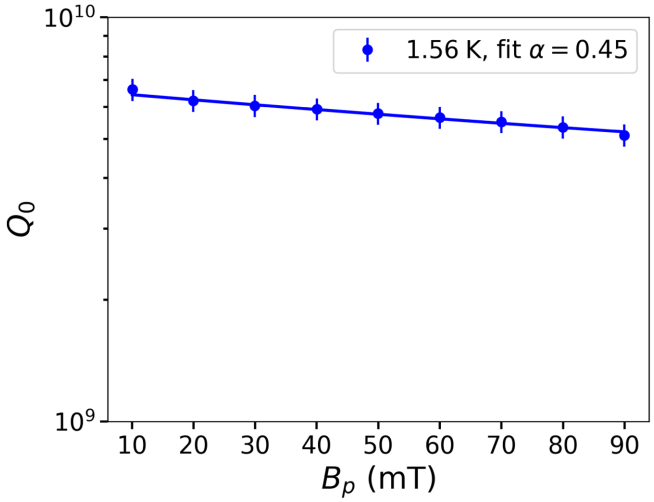

FIG. 11. Fitting of α in Eq. (12) to the Q-curve beginning from the lowest temperature point shown in Fig. 10.

initially (Fig. 10), but the BCS parameters A and Δ_0 are modified to match the BCS resistance appropriate to the Q-curve. All Q-curves measured during a cooldown have B_p starting at 10 mT and increasing in increments of 10 mT. At each B_p, a quality factor $Q_0(B_p)$ is measured at the bath temperature $T_0(B_p)$. Assuming that the 10 mT point is unaffected by field-dependence and TFB, the zero-field BCS resistance is extracted from the 10 mT measurement by

$$R_{\mathrm{BCS}}[T_0(10\ \mathrm{mT})] = \frac{G}{Q_0(10\ \mathrm{mT})} - R_0. \qquad (14)$$

The BCS resistance of the Q-curve will stay close to the value given by Eq. (14) but will deviate from this value both because of TFB and because the helium bath is continuously cooling down during all Q-curve measurements. To find the temperature-dependent $R_{\mathrm{BCS}}(\omega, T)$, the parameters A and Δ_0 in Eq. (12) are fit to the 10 mT data while keeping R_0 fixed. The fitting is done with the constraint that the fit must match the actual Q_0 value for the 10 mT point in the current Q-curve. This ensures that $R_{\mathrm{BCS}}[T_0(10\ \mathrm{mT})]$ from the fit agrees with the value in Eq. (14).

After fitting with this constraint, all parameters except γ in Eq. (12) are determined. The finite-element model can be used to fit γ to the Q-curve with or without accounting for TFB. In the latter case, the rf surface temperature is set to $T = T_0$ everywhere and the fit extracts a value of γ that parametrizes the observed field dependence. When the finite-element model is set to account for TFB, the resulting γ corresponds to the intrinsic field dependence in the Q-curve.

Figure 12 (upper) shows an example of fitting γ to a Q-curve near 4 K. Because TFB causes the surface resistance to increase approximately with the square of the rf field, the shape of the fit curve is not affected by whether TFB is included in the fitting routine. Thus both the fit with and without TFBs are represented by a single curve (solid red) in Fig. 12 (upper). Note that the intrinsic γ is lower than the γ fit without TFB since some portion of the observed field dependence is caused by TFB. The intrinsic γ value can be used to recalculate the data in the curve to simulate how much higher the quality factors would be without TFB, which is shown by the dashed blue curve in Fig. 12 (upper). After recalculating with TFB removed, a significant amount of field dependence remains in the curve shown in Fig. 12 (upper). This trend is seen in all 4 K curves in the coaxial cavity dataset, implying that field dependence at 4 K is primarily due to intrinsic mechanisms rather than TFB.

The same analysis was repeated for Q-curves measured at 2 K, as shown in Fig. 12 (lower). Instead of using the boiling curve fits from Eq. (7), the cooling is described by $q = h_{\mathrm{K}}\Delta T_s$, where a Kapitza conductance value of $h_{\mathrm{K}} = 6700\ \mathrm{W/m^2/K}$ is used [16]. Due to the enhanced

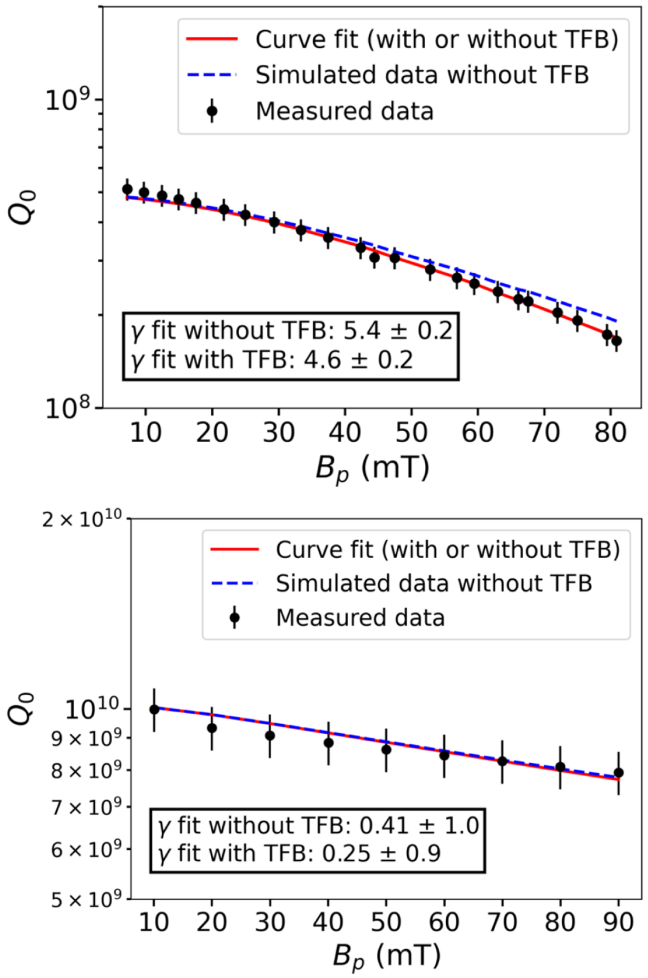

FIG. 12. Q-curves at 4.2 K for the 778 MHz mode of the 300°C baked HWR (upper) and 2.0 K for the 1166 MHz mode of the 400°C baked HWR (lower). The solid red curves show the fit of Eq. (12) to the data. The dashed blue curve shows the red fit curve recalculated with TFB effects removed. In normal fluid helium, the effect of TFB is small but statistically significant, while in superfluid helium it is negligible.

heat transfer as well as the small value of $R_{\mathrm{BCS}}(T)$ at 2 K, TFB is a negligible effect for coaxial cavities operating in superfluid helium. The finite-element model can also predict the rf field amplitude required to bring the maximum surface temperature above T_λ. In principle, this could lead to global thermal runaway and quench due to the change in heat transfer regime, but finite-element calculations showed that the required rf fields are 1.5–2 times higher than the actual quench fields in coaxial cavity tests.

An analysis of the dependence of γ on the rf frequency and surface treatment in TRIUMF's coaxial test cavities was presented in [40]. As shown above, TFB is a weak effect at 4.2 and 2.0 K so this analysis is not significantly affected by correcting for TFB. To study γ at intermediate temperatures, the process of fitting γ with and without accounting for TFB can be repeated for every Q-curve collected in a cooldown, as shown in Fig. 13. In all coaxial

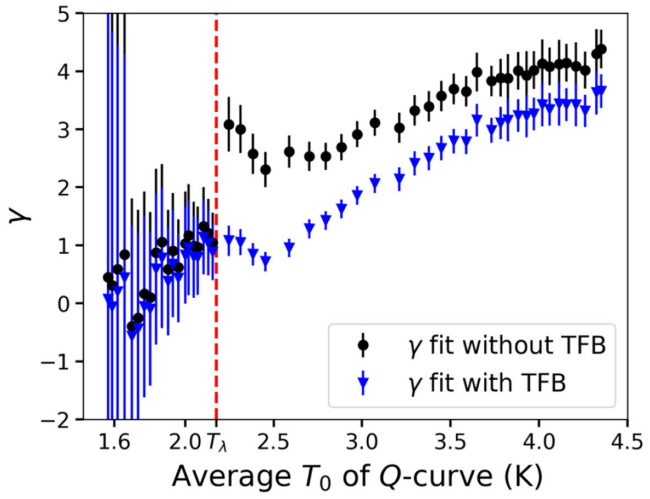

FIG. 13. Fitting of γ in Eq. (12) to all Q-curves in a dataset (778 MHz mode of the 400°C baked HWR). The error bars diverge at low temperatures due to the exponential decay of $R_{\mathrm{BCS}}(T)$ in Eq. (12).

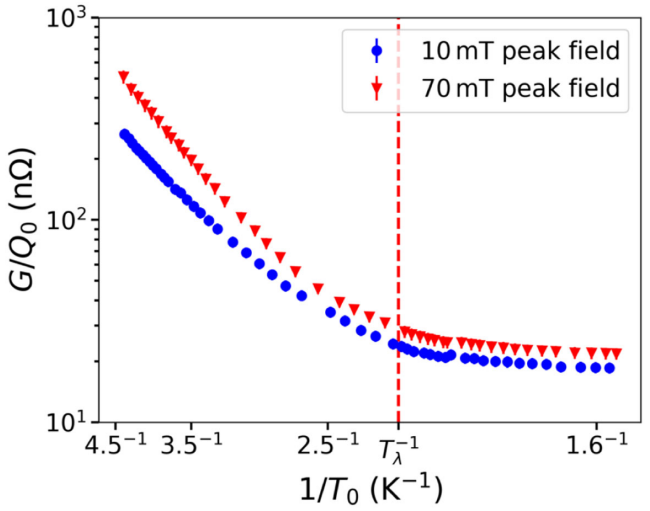

FIG. 14. Data from Fig. 2 recalculated with TFB removed. The jump in surface resistance at T_λ is no longer present.

cavity datasets, it was found that fitting with TFB makes a stronger correction to γ at lower temperatures than at higher temperatures while $T_0 > T_\lambda$. This is because both the thermal conductivity of niobium [Eq. (11)] and the efficiency of heat transfer by boiling (Fig. 6) decrease with temperature. As a result, the correction to γ at temperatures near 4 K is weak, but the TFB correction significantly modifies the temperature dependence of γ. When testing theoretical models that explain the origin of intrinsic field dependence, the TFB correction must, therefore, be taken into account to verify that the model being tested predicts the correct temperature dependence.

Note that in Fig. 13, accounting for TFB does not significantly change the fit value of γ when $T_0 < T_\lambda$. This is the case for all of TRIUMF's coaxial cavity datasets and shows that TFB is a negligible effect for these cavities in the superfluid regime.

In Fig. 13, the γ's fit without TFB are not continuous with the γ's below T_λ. This is a quantitative representation of the change in measured field dependence at the superfluid transition shown in Fig. 2. When the TFB correction is applied in the fitting procedure, the resulting γ's are continuous across T_λ. The TFB fitting correction smooths the discontinuity in γ for all coaxial cavity datasets. This strongly implies that the finite-element model accounts for TFB correctly, since the intrinsic field dependence of the surface resistance should not depend on the helium cooling regime.

After using the TFB model to extract the intrinsic field-dependence parameters from a Q-curve, the model can be used to recompute the Q_0 values in the Q-curve with the effects of TFB removed as was shown in Fig. 12. The process of recalculating the measured data to remove TFB can be repeated for every Q-curve in a coaxial cavity dataset. Figure 14 shows the results of applying this correction to the dataset shown in Fig. 2. For all coaxial cavity datasets, the high-field surface resistance is continuous at T_λ after the TFB correction, which is another way of representing the smoothing of γ shown in Fig. 13.

V. CONCLUSIONS

The methods presented in this study precisely quantify the effect of TFB on coaxial cavity data using a rich new dataset of Nb-LHe boiling curves. The finite-element model developed in this study allows for the creation of a fitting routine that extracts parameters related to field dependence while accounting for TFB as a distinct physical effect to reveal the intrinsic field dependence.

SRF cavities are generally operated at helium bath temperatures of either 4.2 or below 2.0 K. Because TFB was found to only weakly affect field dependence at these temperatures, improving the boiling performance of a coaxial cavity through treatments to the external surface of the cavity will not lead to significant gains in quality factor. However, this conclusion does not necessarily hold for elliptical cavities operated at or above 1.3 GHz, where the higher BCS resistance may lead to stronger thermal effects.

The primary purpose of the methods developed in this study is to aid in fundamental studies of field dependence. Our results suggest that future studies of field dependence in coaxial cavities can safely neglect TFB at bath temperatures of 4.2 and 2.0 K. However, at intermediate temperatures, TFB has a stronger effect and where cooldown data are used to extract fundamental parameters like R_{BCS} and R_0, considerations of TFB are essential.

ACKNOWLEDGMENTS

The authors would like the thank the technical team in TRIUMF's SRF group, in particular Devon Lang, James

Kier, Bhalwinder Waraich, Ruminder Sekhon, and Ben Matheson, as well as the cryogenics team, namely David Kishi, Rowan Bjarnesson, and Johnson Cheung, for their assistance in conducting experiments. This work was supported by the Natural Sciences and Engineering Research Council of Canada (NSERC) through Grant No. SAPIN-2019-00040.

[1] J. Dilling, R. Krücken, and G. Ball, ISAC overview, Hyperfine Interact. **225**, 1 (2014).
[2] M. Leitner, The FRIB project at MSU, in *Proceedings of the International Conference on RF Superconductivity, Paris, France* (JACOW, Geneva, Switzerland, 2013).
[3] J. Galayda, The LCLS-II: A high power upgrade to the LCLS, in *Proceedings of the 9th International Particle Accelerator Conference, IPAC-2018, Vancouver, BC, Canada* (2018), MOYGB2, pp. 18–23.
[4] The European X-Ray Free-Electron Laser—Technical Design Report, DESY, Technical Report No. DESY 2006-097, 2007.
[5] D. C. Mattis and J. Bardeen, Theory of the anomalous skin effect in normal and superconducting metals, Phys. Rev. **111**, 412 (1958).
[6] J. Halbritter, Comparison between measured and calculated RF losses in the superconducting state, Z. Med. Phys. **238**, 466 (1970).
[7] A. Gurevich, Theory of RF superconductivity for resonant cavities, Supercond. Sci. Technol. **30**, 034004 (2017).
[8] A. Grassellino, A. Romanenko, D. Sergatskov, O. Melnychuk, Y. Trenikhina, A. Crawford, A. Rowe, M. Wong, T. Khabiboulline, and F. Barkov, Nitrogen and argon doping of niobium for superconducting radio frequency cavities: A pathway to highly efficient accelerating structures, Supercond. Sci. Technol. **26**, 102001 (2013).
[9] S. Posen, A. Romanenko, A. Grassellino, O. Melnychuk, and D. Sergatskov, Ultralow surface resistance via vacuum heat treatment of superconducting radio-frequency cavities, Phys. Rev. Appl. **13**, 014024 (2020).
[10] S. Posen *et al.*, High gradient performance and quench behavior of a verification cryomodule for a high energy continuous wave linear accelerator, Phys. Rev. Accel. Beams **25**, 042001 (2022).
[11] W. Weingarten, Field-dependent surface resistance for superconducting niobium accelerating cavities, Phys. Rev. ST Accel. Beams **14**, 101002 (2011).
[12] T. Kubo and A. Gurevich, Field-dependent nonlinear surface resistance and its optimization by surface nanostructuring in superconductors, Phys. Rev. B **100**, 064522 (2019).
[13] H. Padamsee, *RF Superconductivity: Science, Technology, and Applications, RF Superconductivity* (Wiley, New York, NY, 2009).
[14] M. McMullin, T. Junginger, P. Kolb, R. Laxdal, and Z. Yao, Thermal feedback in coaxial SRF cavities, in *Proceedings of the 21st International Conference on RF Superconductivity, Grand Rapids, MI* (JACOW, Geneva, Switzerland, 2023).
[15] K. Mittag, Kapitza conductance and thermal conductivity of copper niobium and aluminium in the range from 1.3 to 2.1 K, Cryogenics **13**, 94 (1973).
[16] J. Amrit and M. X. François, Heat flow at the niobium-superfluid helium interface: Kapitza resistance and superconducting cavities, J. Low Temp. Phys. **119**, 27 (2000).
[17] P. Bauer, N. Solyak, G. Ciovati, G. Eremeev, A. Gurevich, L. Lilje, and B. Visentin, Evidence for non-linear BCS resistance in SRF cavities, Phys. C **441**, 51 (2006).
[18] J. Ding, D. Hall, and M. Liepe, Simulations of RF field-induced thermal feedback in niobium and Nb_3Sn cavities, in *Proceedings of the 18th International Conference on RF Superconductivity, SRF2017, Lanzhou, China* (JACoW, Geneva, Switzerland, 2018), THPB079.
[19] R. Cummings and J. Smith, Boiling heat transfer to liquid helium, in *Pure and Applied Cryogenics* (Elsevier, Oxford, 1966), Vol. 6, pp. 85–95.
[20] M. D. Reeber, Heat transfer to boiling helium, J. Appl. Phys. **34**, 481 (1963).
[21] K. R. Krafft, Thermal transport and thermal-magnetic breakdown in superconducting cavities made of high thermal conductivity niobium, Ph.D. thesis, Cornell University, 1983.
[22] J. Vines, Y. Xie, and H. Padamsee, Systematic trends for the medium field Q-slope, in *Proceedings of the 13th International Workshop on RF Superconductivity, SRF-2007, Beijing, China* (Peking University, Beijing, China, 2007).
[23] G. Ciovati, P. Dhakal, and A. Gurevich, Decrease of the surface resistance in superconducting niobium resonator cavities by the microwave field, Appl. Phys. Lett. **104**, 092601 (2014).
[24] P. Kolb, Z. Yao, T. Junginger, B. Dury, A. Fothergill, M. Vanderbanck, and R. E. Laxdal, Coaxial multimode cavities for fundamental superconducting rf research in an unprecedented parameter space, Phys. Rev. Accel. Beams **23**, 122001 (2020).
[25] V. Palmieri, A. A. Rossi, S. Y. Stark, and R. Vaglio, Evidence for thermal boundary resistance effects on superconducting radiofrequency cavity performances, Supercond. Sci. Technol. **27**, 085004 (2014).
[26] M. Jergel and R. Stevenson, Static heat transfer to liquid helium in open pools and narrow channels, Int. J. Heat Mass Transfer **14**, 2099 (1971).
[27] S. W. Van Sciver, *Helium Cryogenics* (Springer US, Boston, MA, 1986).
[28] S. H. Carpenter and R. H. Wittman, Explosion welding, Annu. Rev. Mater. Sci. **5**, 177 (1975).
[29] M. Fouaidy, Thermal conductivity of niobium and thermally sprayed copper at cryogenic temperature, IOP Conf. Ser. Mater. Sci. Eng. **1241**, 012012 (2022).
[30] I. Pioro, W. Rohsenow, and S. Doerffer, Nucleate pool-boiling heat transfer. I: Review of parametric effects of boiling surface, Int. J. Heat Mass Transfer **47**, 5033 (2004).
[31] Cernox®, https://www.lakeshore.com/products/categories/overview/temperature-products/cryogenic-temperature-sensors/cernox.
[32] F. Koechlin and B. Bonin, Parametrization of the niobium thermal conductivity in the superconducting state, Supercond. Sci. Technol. **9**, 453 (1996).

[33] V. Palmieri and R. Vaglio, Thermal contact resistance at the Nb/Cu interface as a limiting factor for sputtered thin film RF superconducting cavities, Supercond. Sci. Technol. **29**, 015004 (2016).

[34] N. Kaneyasu, F. Yasunobu, U. Satoru, and O. Haruhiko, Effect of surface configuration on nucleate boiling heat transfer, Int. J. Heat Mass Transfer **27**, 1559 (1984).

[35] M. McMullin, Thermal feedback in coaxial superconducting RF cavities, MSc thesis, University of Victoria, 2023.

[36] A. C. Polycarpou, *Introduction to the Finite Element Method in Electromagnetics*, Synthesis Lectures on Computational Electromagnetics (Springer, New York, 2005), Vol. 1.

[37] T. P. Sheahen, Rules for the energy gap and critical field of superconductors, Phys. Rev. **149**, 368 (1966).

[38] A. Miyazaki and W. V. Delsolaro, Two different origins of the Q-slope problem in superconducting niobium film cavities for a heavy ion accelerator at CERN, Phys. Rev. Accel. Beams **22**, 073101 (2019).

[39] A. Gurevich, Multiscale mechanisms of SRF breakdown, Phys. C **441**, 38 (2006).

[40] P. Kolb, Z. Yao, A. Blackburn, R. Gregory, D. Hedji, M. McMullin, T. Junginger, and R. E. Laxdal, Mid-T heat treatments on BCP'ed coaxial cavities at TRIUMF, Front. Electron. Mater. **3**, 1244126 (2023).